

A Controller Improving Photovoltaic Voltage Regulation in the Single-Stage Single-Phase Inverter

Leonardo Callegaro[✉], Member, IEEE, Christian A. Rojas[✉], Senior Member, IEEE,
Mihai Ciobotaru[✉], Senior Member, IEEE, and John E. Fletcher[✉], Senior Member, IEEE

Abstract—While substantial research covers current control and synchronization of grid-connected photovoltaic (PV) inverters, issues concerning control of the PV input voltage deserve more attention, as they equally affect the reliable and stable operation of the system. Hence, this article analyses the PV voltage regulation in the single-stage single-phase PV inverter. In contrast to previous work, the PV source influence on the input voltage dynamic is analytically formalized, exposing a potential instability when the PV source is operating in its constant current region. A traditional proportional-integral PV voltage controller fails to ensure a consistent and stable voltage regulation. On the other hand, this issue is resolved by the proposed feedback linearization based controller. The new controller is validated on a test setup comprising of a PV source emulating a 1.2 kW PV array, interfaced to a single-phase inverter connected to a grid emulator. Confirming the issues predicted by the theoretical analysis, the experiments prove two main advantages of the proposed controller. First, PV voltage regulation instability is eliminated when the PV array operates in its constant current region. Second, the PV voltage transient behavior is now independent of the operating point of the PV source.

Index Terms—Cascaded control, dc-ac power conversion, photovoltaic (PV) power systems, PV voltage control, transient response.

I. INTRODUCTION

THE electricity sector is going through a green revolution, powered by the uptake of renewables and retirement of fossil-fuel-based generation. In this scenario, solar photovoltaic (PV) systems are among the largest contributors to the renewable energy mix, thanks to the key role of power electronic converters.

Manuscript received January 11, 2021; revised April 8, 2021 and June 11, 2021; accepted July 17, 2021. Date of publication July 27, 2021; date of current version September 16, 2021. This work was supported in part by Macquarie University ECR Enabling Scheme 2021, under Grant 168590913, and in part by ARENA, under Grant G00865. The work of Christian A. Rojas was supported by ANID/Fondecyt Regular under Grants 1210757, ANID/FB0008, and ANID/FONDAP/15110019. Recommended for publication by Associate Editor S. A. Khajehoddin. (*Corresponding author: Leonardo Callegaro.*)

Leonardo Callegaro is with the School of Engineering, Macquarie University, Sydney, NSW 2109, Australia (e-mail: leonardo.clgr@gmail.com).

Christian A. Rojas is with the Electronics Engineering Department, Universidad Técnica Federico Santa María, Valparaíso 2390123, Chile (e-mail: c.a.rojas@ieee.org).

Mihai Ciobotaru is with EcoJoule Energy, Brisbane, QLD 4131, Australia (e-mail: ciomih@ieee.org).

John E. Fletcher is with the School of Electrical Engineering and Telecommunications, The University of New South Wales, Sydney, NSW 2052, Australia (e-mail: john.fletcher@unsw.edu.au).

Color versions of one or more figures in this article are available at <https://doi.org/10.1109/TPEL.2021.3100530>.

Digital Object Identifier 10.1109/TPEL.2021.3100530

Modeling and control of converters is an established yet ever-growing topic among industrial and academic circles, which initially focused on dc–dc converters and then delved into dc–ac converters. Despite the early achievements, small-signal models of dc–dc converters were formally revisited in the presence of a PV input only in the mid 2000s. In [1] and [2], it was found that the dynamic resistance of the PV source heavily affects the converter transient performance and PV voltage regulation. Later, the authors in [3]–[8] revealed stability issues in PV interfacing current-controlled buck converters caused by the variability of dynamic and static resistance of the PV source.

Due to the sinusoidal nature of the output variables, small-signal models of dc–ac voltage source inverters (VSI) cannot be derived directly from average equations, like in dc–dc converters. The dq transformation solves this problem for the three-phase VSI, permitting to analyze it as two (cross-coupled) dc–dc converters, one for the d -axis, and one for the q -axis. Adopting this modeling framework, the influence of the PV source on the stability of three-phase VSIs was mathematically formulated in [9], [10], similarly to dc–dc converters. Again, it was found that the operating point on the PV source affects the quality and stability of the PV voltage regulation. In the single-phase domain, applying the dq transformation requires creating an artificial orthogonal component of the grid voltage, which introduces delays, and worsens the dynamic performance of the control loops. Although [11] and [12] proposed techniques such as *fictive-axis emulation* and *fast orthogonal signal generation* to overcome these issues, dq frame control and modeling of single-phase inverters is generally more complicated compared with three-phase systems and therefore, in alignment with [13, p. 189], it is here avoided.

Controller design for grid-connected single-phase PV inverters is usually carried out by studying the outer voltage loop and the inner current loop independently, given their large difference in bandwidth [14]. While the fast current controller is designed around the transfer function of the filter between the inverter and the grid, the slow PV voltage controller is designed disregarding the fast current loop dynamic. For the single-stage single-phase PV inverter of Fig. 1, the available literature does not provide a small-signal model of the dc voltage dynamic taking into account the intrinsic properties of the PV source. In [15] for instance, there is no mention of the model used to design the PV voltage controller. In [9], [10], and [16], despite studying in-depth various PV interfacing converters, the topology of Fig. 1 is not considered. Controller design based on dc-link capacitor energy

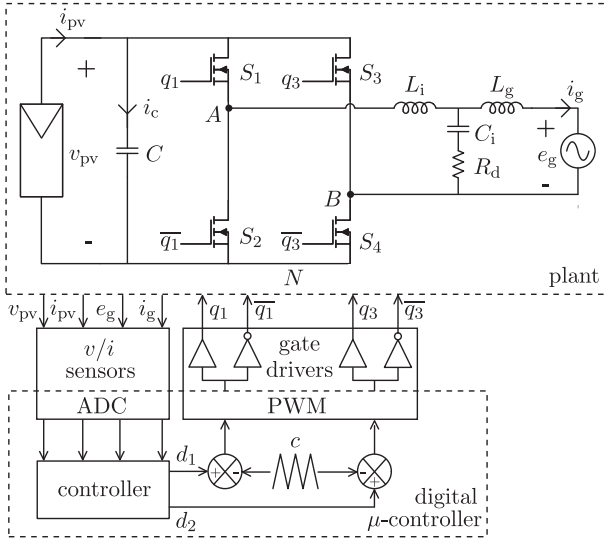


Fig. 1. Single-stage single-phase PV inverter power stage and control diagram.

balancing is presented in [17], albeit focusing on double-stage single-phase PV inverters, and without discussing the dynamic model of the PV source. In [18], which deals with several control issues of single-stage single-phase PV inverters, the impact of the PV source on the dc input voltage regulation was not treated. In [19, pp. 192–193], the dc input voltage dynamic of the single-stage single-phase PV inverter is modeled considering the power balance on the input capacitor, but without including the PV source parameters in the model. These considerations highlight an apparent gap in the existing knowledge: There is a need to formalize the impact of the PV source on the input voltage dynamic of the single-stage single-phase inverter.

Bridging such a gap, this article demonstrates that the transfer function modeling the PV voltage behavior is not only dependent on the input capacitor, but is also heavily affected by the PV source operating point. Operation outside the maximum power point (MPP) is often required in practice, where PV inverters periodically sweep the I - V curve to track the global MPP [20], or curtail their power to support the grid during over-frequency events, e.g., by moving the PV voltage reference to the left of the MPP [21], [22]. This article shows that when the PV source operating point is in the current source region, i.e., on the left of the MPP, traditional controllers can fail to regulate the inverter input voltage, with detrimental effects on PV voltage stability and transient performance. To solve these issues, a new PV voltage controller based on feedback linearization is proposed, and it has two main benefits. First, it eliminates possible PV voltage instability caused by the dynamic behavior of the PV source, increasing the system robustness. Second, it desirably makes the PV voltage regulation independent of the PV source operating point.

The next section derives a complete model for the inverter input voltage control, taking into account the properties of the PV source. Section III exposes the limitations of a traditional PV voltage controller and proposes a new controller design to address them. In Section IV and V, the issues predicted by theoretical analysis are verified through simulations and experiments,

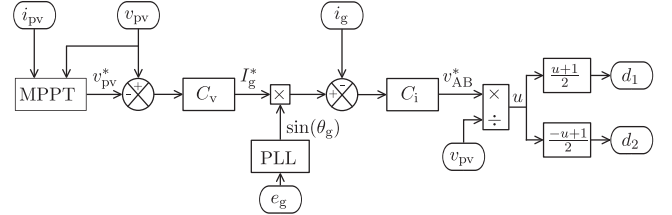


Fig. 2. Traditional cascaded control scheme for PV voltage and grid current regulation (represents the content of the “controller” block in Fig. 1).

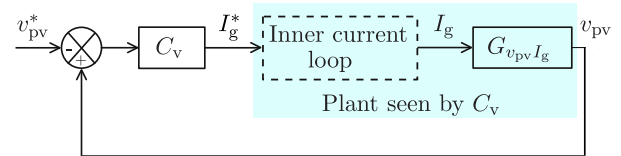


Fig. 3. Traditional framework for designing the voltage controller, C_v ; the inner current loop is considered a unity gain due to its fast dynamic, i.e., $I_g = I_g^*$, and the plant seen by C_v is reduced to $G_{v_{pv}I_g}$.

respectively. The conditions causing PV voltage instability in the current source region of the PV source are exposed, and the performance advantages of the proposed controller are thoroughly evaluated. Section VI concludes this article, summarizing its main results and contribution.

II. PV SOURCE AFFECTED DC INPUT VOLTAGE DYNAMIC

The single-stage single-phase PV inverter schematic is shown in Fig. 1. Grid current harmonics are minimized through a passively damped LCL filter, with this solution chosen due to its simplicity. At low frequencies, the damped LCL filter is approximated by its inductive component [23], $L \approx L_i + L_g$, permitting to write a simplified switching cycle averaged state-equation (1a) for the ac side of the inverter. The averaged model is completed by the capacitor current state-equation (1b) for the inverter PV side. It is

$$\dot{i_L} = v_{AB} - e_g = v_{pv}u - e_g \quad (1a)$$

$$\dot{Cv}_{pv} = i_{pv} - i_L u. \quad (1b)$$

The modulation index $u \in [-1, 1]$ is the control input in (1a) and (1b), and can equally be written in terms of the upper switches (S_1, S_3) duty cycle, d_1, d_2 , with $d_1, d_2 \in [0, 1]$.

A common scheme to regulate the PV voltage and grid current in the circuit of Fig. 1 is the cascaded controller of Fig 2. A fast inner loop regulates the grid current by setting the inverter modulation index u (hence d_1, d_2), and has a typical bandwidth of few hundred Hz, e.g., 500 Hz in [15]. A slow outer loop regulates the PV voltage to track the value calculated by a maximum power point tracking (MPPT) algorithm, setting the peak grid current reference, I_g^* , for the inner loop. For the current controller to track the reference set by the voltage controller, the bandwidth of the two loops is usually designed to be one decade apart [14, p. 564]. In other words, the actual peak grid current is considered equal to its reference when designing the PV voltage controller [18]. With this hypothesis, $I_g = I_g^*$, the inner current loop in Fig. 3 is a unity gain, and the voltage controller C_v is designed around the plant $G_{v_{pv}I_g}$. The voltage loop bandwidth

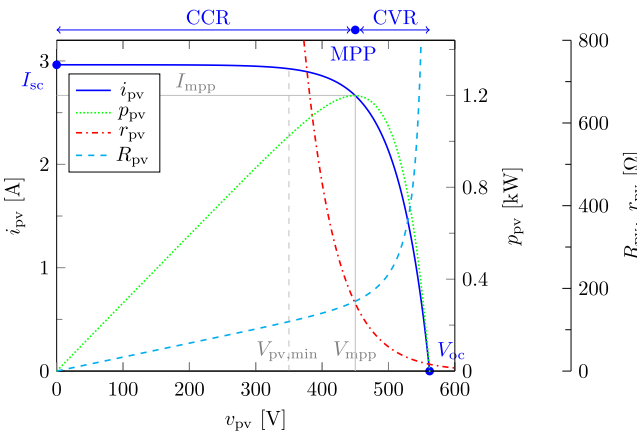


Fig. 4. Characteristic current, power, and resistance curves of a PV source (at 1 kW/m² and 25 °C), and identification of constant current region (CCR), maximum power point (MPP), and constant voltage region (CVR).

is usually tens of Hz, and in practice is ranging only from a few Hz [10] to 20 Hz [24]. A low value is used to suppress the double line frequency ripple propagating from the dc input to the grid current reference.

Applying the average power balance on the input capacitor and disregarding converter losses for simplicity, the average power entering the inverter from the dc port, P_{dc} , equals the average power injected into the grid, P_g , therefore

$$P_{pv} - P_g = P_c. \quad (2)$$

P_{pv} is the average power output from the PV source. P_c is the average power through the input capacitor, responsible for linear variations of the capacitor voltage when the input power P_{pv} differs from P_g . The latter is the dc component of the instantaneous ac power injected into the grid, p_g . Indicating peak values of grid voltage and current with E_g and I_g , respectively, and assuming unity power factor operation, it is

$$p_g = E_g \sin(\theta_g) I_g \sin(\theta_g) = \frac{E_g I_g}{2} (1 - \cos(2\theta_g)) \quad (3)$$

in which $\frac{E_g I_g}{2} = P_g$. Thus, (2) is rewritten as

$$v_{pv} i_{pv} - \frac{E_g I_g}{2} = v_{pv} C \dot{v}_{pv} \quad (4)$$

where $i_c = C \dot{v}_{pv}$ is the input capacitor current. Finally, (4) can be perturbed and linearized about a steady-state operating point, yielding the small-signal relation

$$\tilde{v}_{pv} I_{pv} + V_{pv} \tilde{i}_{pv} - \frac{\tilde{E}_g I_g}{2} - \frac{E_g \tilde{I}_g}{2} = V_{pv} C \tilde{v}_{pv} \quad (5)$$

where small-signal variations are indicated by a tilde ($\tilde{\cdot}$).

Static resistance and small-signal dynamic resistance of the PV source in a quiescent point (V_{pv}, I_{pv}) [8], [9], [25] are defined respectively as

$$R_{pv} = \frac{V_{pv}}{I_{pv}}, \quad r_{pv} = -\left. \frac{\partial v_{pv}}{\partial i_{pv}} \right|_{\substack{v_{pv}=V_{pv} \\ i_{pv}=I_{pv}}} = -\frac{\tilde{v}_{pv}}{\tilde{i}_{pv}}. \quad (6)$$

Given a PV source characteristic such as in Fig. 4, static and dynamic resistance vary considerably depending on the

quiescent point. Using (6) in (5), yields the sought-after transfer function of the plant seen by the voltage controller

$$G_{v_{pv} I_g}(s) = \left. \frac{\tilde{v}_{pv}}{\tilde{I}_g} \right|_{\tilde{E}_g=0} = \frac{-E_g}{2V_{pv}C \left[s + \frac{1}{C} \left(\frac{1}{r_{pv}} - \frac{1}{R_{pv}} \right) \right]}. \quad (7)$$

Small-signal transfer function (7) represents a simple yet powerful result. In fact, as R_{pv} and r_{pv} vary widely depending on the PV source quiescent point, on the left of the MPP, where $r_{pv} > R_{pv}$, the pole in (7) moves to the right half plane (RHP), highlighting that the plant seen by the voltage controller becomes unstable. Such plant instability is otherwise hidden when the PV source is operated on the right of the MPP (constant voltage region), where $r_{pv} < R_{pv}$, and at the MPP, where $r_{pv} = R_{pv}$ (see Fig. 4). Finally, if the voltage controller were designed only considering MPP operation, where $r_{pv} = R_{pv}$, then (7) would be reduced to $G_{v_{pv} I_g} = \frac{-E_g}{2V_{pv}C s}$ as in [19, pp. 192–193], which hides the plant instability appearing in the constant current region of the PV source.

The next section investigates the closed-loop stability of the PV voltage regulation system, considering that the plant seen by the voltage controller is intrinsically unstable when the PV source operates in the constant current region.

III. PV VOLTAGE CONTROLLER DESIGN

A. Traditional Control Scheme

In the cascaded control scheme of Fig. 2, the low bandwidth of the outer PV voltage loop justifies approximating the fast inner current loop as a unity gain ($\frac{I_g}{I_g^*} = 1$). Therefore, closed-loop PV voltage regulation stability is studied based on the scheme of Fig. 3, where (7) is the plant seen by the voltage controller, unstable at the left of the MPP, where $r_{pv} > R_{pv}$. Stability of the system in Fig. 3 is ensured if its closed-loop transfer function

$$G_{v_{pv,cl}}(s) = \frac{\tilde{v}_{pv}}{\tilde{v}_{pv}^*} = \frac{-C_v(s) G_{v_{pv} I_g}(s)}{1 - C_v(s) G_{v_{pv} I_g}(s)} \quad (8)$$

has no RHP poles. Hence, using a proportional-integral (PI) voltage controller $C_v(s) = k_{pv} + \frac{k_{iv}}{s}$, closed-loop stability is granted if the denominator of (8), $D(s)$, has no RHP roots. It is

$$D(s) = s^2 + s (\omega_p - k_{pv} K) - k_{iv} K \quad (9)$$

$$K = \frac{-E_g}{2V_{pv}C}, \quad \omega_p = \frac{1}{C} \left(\frac{1}{r_{pv}} - \frac{1}{R_{pv}} \right) \quad (10)$$

where the gain and angular frequency of the pole in (7), respectively, are given in (10). If all coefficients of s in (9) are positive, then the roots of $D(s)$ lie in the left half of the complex plane (LHP), and the closed-loop system (8) is stable [26, p. 394]. This condition is satisfied as long as the coefficient of s in (9) is positive, i.e., $\omega_p - k_{pv} K > 0$, which, using (10), translates to a constraint on the proportional gain of the PV voltage controller

$$k_{pv} > -\frac{2V_{pv}}{E_g} \left(\frac{1}{r_{pv}} - \frac{1}{R_{pv}} \right). \quad (11)$$

Since the proportional gain, k_{pv} , is positive, constraint (11) is satisfied whenever the PV source operates in the constant voltage

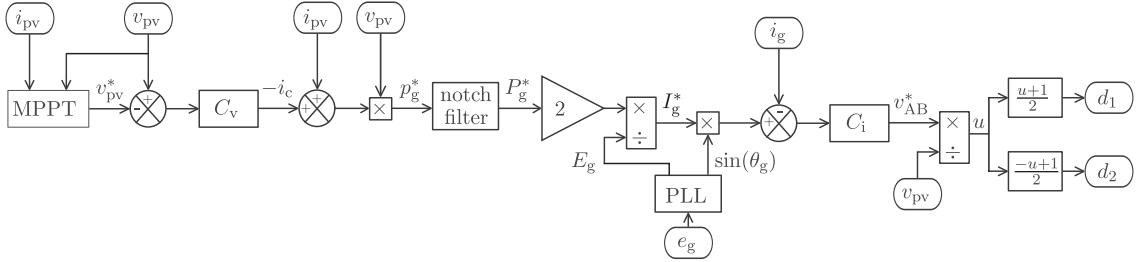


Fig. 5. Proposed cascaded control scheme for PV voltage and grid current (represents the content of the “controller” block in Fig. 1).

region (on the right of the MPP), where $R_{\text{pv}} > r_{\text{pv}}$, and the right hand side term in (11) is negative. At the MPP, where $R_{\text{pv}} = r_{\text{pv}}$, the system is also stable as (11) is satisfied. Conversely, when the PV source is in the constant current region (on the left of the MPP), where $r_{\text{pv}} > R_{\text{pv}}$, the right hand side term in (11) is positive, and k_{pv} needs to be greater than this positive value to ensure closed-loop stability. The right hand side term in (11) is positive, and highest, when $r_{\text{pv}} \gg R_{\text{pv}}$, therefore $\frac{1}{r_{\text{pv}}} \rightarrow 0$ and $\frac{1}{R_{\text{pv}}} \approx \frac{I_{\text{sc}}}{V_{\text{pv},\text{min}}}$, i.e., the PV source is operating in the constant current region at its minimum voltage, $V_{\text{pv},\text{min}}$, and short-circuit current, I_{sc} (see Fig. 4). Closed-loop stability is preserved in this worst case PV operating condition, if

$$k_{\text{pv}} > k_{\text{safety}} \frac{2V_{\text{pv}}I_{\text{sc}}}{E_g V_{\text{pv},\text{min}}} \quad (12)$$

where a factor, e.g., $k_{\text{safety}} = 2$, is introduced for safety.

Condition (12) is equivalent to tuning the voltage controller so that the voltage loop cross-over frequency (or bandwidth), ω_v , is at least twice the frequency of the worst-case RHP pole, [10], [27], [28]. This requirement translates into

$$\omega_v > 2 \max \left| \frac{1}{C} \left(\frac{1}{r_{\text{pv}}} - \frac{1}{R_{\text{pv}}} \right) \right| = 2 \frac{I_{\text{sc}}}{CV_{\text{pv},\text{min}}} \quad (13)$$

which considers the worst-case scenario when the PV operating point is in the constant current region at $V_{\text{pv},\text{min}}, I_{\text{sc}}$. The loop-gain [29, p. 241] of the PV voltage loop in Fig. 3 is

$$T_v(s) = C_v(s) G_{v_{\text{pv}} I_g}(s). \quad (14)$$

At the cross-over frequency, ω_v , $|T_v(j\omega_v)| = 1$ and being ω_v far removed from the pole frequency of (7), then $|T_v(j\omega_v)| \approx \frac{k_{\text{pv}} E_g}{2V_{\text{pv}} C \omega_v}$, yielding in $\omega_v = \frac{k_{\text{pv}} E_g}{2V_{\text{pv}} C}$, which substituted in (13) results in the constraint for k_{pv} to avoid closed-loop instability

$$k_{\text{pv}} > \frac{4V_{\text{pv}} C \omega_{\text{RHP}}}{E_g}, \quad \omega_{\text{RHP}} = \frac{I_{\text{sc}}}{CV_{\text{pv},\text{min}}} \quad (15)$$

where ω_{RHP} is the worst-case RHP frequency of the pole in (7). Condition (15) for k_{pv} , derived around the bandwidth of the PV voltage loop, is therefore identical to condition (12), determined by studying the stability of the closed-loop system (8). Finally, the voltage controller integral gain, k_{iv} , is chosen to ensure that there is no phase delay caused by the integrator at ω_v , thus posing the PI zero, located at $\frac{k_{iv}}{k_{\text{pv}}}$, no less than one decade far from ω_v , yielding

$$k_{iv} \leq 0.1 k_{\text{pv}} \omega_v. \quad (16)$$

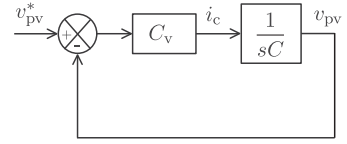


Fig. 6. Block diagram used for designing the PV voltage PI controller.

In summary, closed-loop stability of the traditional PV voltage regulation scheme (Figs. 2 and 3) is undesirably dependent on the value of PI controller proportional gain, k_{pv} . In the constant current region of the PV source, an insufficient value of k_{pv} , would result in the violation of (12), with detrimental effects on the PV voltage regulation. This issue is overcome with the control technique proposed next.

B. Proposed Control Based on Feedback Linearization

The proposed control scheme is portrayed in Fig. 5. As before, design of the proposed PV voltage controller assumes the inner current loop to be much faster than the outer voltage loop. In other words, the measured grid current, i_g , equals its reference, i_g^* , at all times, noting that $i_g^* = I_g^* \sin(\theta_g)$, and the closed-loop dynamic of the current loop does not affect the voltage loop dynamic. Therefore, the current controller remains the same as in the traditional control scheme. The scope of the outer voltage loop is still to provide the peak value of the grid current reference, I_g^* , to the inner current loop. However, in the proposed PV voltage controller, I_g^* is not the direct output of the voltage PI (as in Fig. 2), as elaborated in the next paragraph.

The instantaneous power balance on the input capacitor is

$$p_{\text{pv}} - p_g = p_c \quad (17)$$

the capacitor current, i_c , can be expressed rewriting (17) as

$$i_{\text{pv}} - \frac{p_g}{v_{\text{pv}}} = i_c. \quad (18)$$

Choosing the capacitor current $i_c = C \dot{v}_{\text{pv}}$ as the new outer loop control variable, this is the output of a linear controller, $C_v(s)$, simply designed around the plant $G_v(s) = \frac{v_{\text{pv}}}{i_c} = \frac{1}{sC}$ (Fig. 6), so that

$$i_c = C_v(s)(v_{\text{pv}}^* - v_{\text{pv}}). \quad (19)$$

The new control variable, i_c , allows to design a PI controller $C_v(s)$ regulating the PV voltage, however, the actual control input to the inner current loop, I_g^* , must still be derived. Pursuing

this objective, the instantaneous power injected into the grid is

$$p_g = v_{\text{pv}} (i_{\text{pv}} - i_c) \quad (20)$$

where i_c is from (19). The dc component, P_g , can be extracted from (20) by eliminating the double line frequency ripple component. Therefore, the term on the right hand side of (20) is passed through a notch filter, tuned to eliminate the double line frequency. Hence, the peak grid current reference, I_g^* , is calculated from the average ac power, P_g^* , available at the output of the notch filter. Finally, using the dc term of (3), and reminding that for the voltage loop $I_g^* = I_g$, the ac peak current reference for the inner loop is

$$I_g^* = \frac{2P_g^*}{E_g}. \quad (21)$$

In the proposed control scheme of Fig. 5, the peak grid current reference, I_g^* , is calculated using the output of the PI controller, $C_v(s)$, as well as feed-forward signals from the PV source, v_{pv} and i_{pv} , and the output of a notch filter, P_g^* . The feed-forward signals remove the dependence of the PV voltage regulation on the operating point of the PV source, eliminating the stability issues appearing with the traditional control when the PV source operates in the CCR (Fig. 4). Particularly, the proposed control scheme is closed-loop stable, independently from the value of the PI voltage controller gains. This approach is based on the manipulation of large-signal nonlinear equations, rather than on small-signal transfer functions. Hence, proof of closed-loop stability is given directly in the time domain.

Assuming that the average ac power is unaffected by the unitary-gain notch filter, the proposed control law for I_g^* is

$$\begin{aligned} I_g^* &= \frac{2}{E_g} v_{\text{pv}} [i_{\text{pv}} + k_{\text{pv}} (v_{\text{pv}} - v_{\text{pv}}^*) + k_{\text{iv}} \xi_v] \\ \dot{\xi}_v &= v_{\text{pv}} - v_{\text{pv}}^* \end{aligned} \quad (22)$$

and substituted into the large-signal nonlinear equation (4) describing the PV voltage dynamic, gives

$$v_{\text{pv}} i_{\text{pv}} - v_{\text{pv}} [i_{\text{pv}} + k_{\text{pv}} (v_{\text{pv}} - v_{\text{pv}}^*) + k_{\text{iv}} \xi_v] = v_{\text{pv}} C \dot{v}_{\text{pv}}. \quad (23)$$

Noting from (22) that $\dot{v}_{\text{pv}} = \dot{\xi}_v$ (as v_{pv}^* is considered constant), after some algebra, (23) yields the linear differential equation

$$-k_{\text{pv}} \dot{\xi}_v - k_{\text{iv}} \xi_v = C \ddot{\xi}_v. \quad (24)$$

The characteristic equation associated with (24) is

$$\frac{k_{\text{iv}}}{C} + \frac{k_{\text{pv}}}{C} r + r^2 = 0 \quad (25)$$

and its roots r_1, r_2 , lie in the left half of the complex plane because the coefficients $\frac{k_{\text{iv}}}{C}, \frac{k_{\text{pv}}}{C}$ are positive [26, p. 394].

In conclusion, the proposed nonlinear control law (22) for I_g^* has the benefit of linearizing the large-signal PV voltage dynamic (4), while canceling the nonlinearity of the PV generator. This scheme is closed-loop stable, regardless of the PV generator operating point, and independently of the voltage controller gains. Compared with the traditional control scheme discussed in Section III-A, the outcome of the proposed controller are more robust stability and enhanced PV voltage transient performance, decoupled from the operating point of the PV source. These

TABLE I
INVERTER AND PV SOURCE PARAMETERS

	Parameter	Variable	Value
Inverter	Grid side inductance	L_g	0.5 mH
	Inverter side inductance	L_i	1.3 mH
	Filter capacitance	C_i	4.7 μF
	Damping resistance	R_d	3.3 Ω
	PV side capacitance	C	1.18 mF*
PV source (Fig. 4)	Switching frequency	f_{sw}	10 kHz
	MPP Power	P_{mpp}	1.2 kW
	MPP voltage	V_{mpp}	450 V
	MPP current	I_{mpp}	2.7 A
	Open-circuit voltage	V_{oc}	562 V
	Short-circuit current	I_{sc}	2.9 A

*Additional simulations with $C = 300 \mu\text{F}$ are carried out to verify the influence of this parameter on the controller performance.

benefits are apparent from the simulation and experimental results presented in the next sections.

IV. SIMULATION RESULTS

The system in Fig. 1 was simulated in PLECS to evaluate the transient performance of the traditional (Fig. 2) and proposed (Fig. 5) PV voltage control schemes. Parameters of interest used in the simulation are reported in Table I. The grid voltage was set to $e_g = \sqrt{2} 230 \sin(2\pi 50t)$ V. Synchronization of the inverter with the grid occurs via a phase locked loop (PLL) tailored for single-phase systems [30], implemented as per [31]. The grid current synthesized by the inverter is controlled by a proportional-resonant controller with 3rd, 5th, and 7th harmonic compensation. The inner loop target bandwidth chosen is 500 Hz, much higher than the PV voltage loop bandwidth, so that the current loop dynamic is not affecting the voltage regulation. The current controller is

$$C_i(s) = k_{\text{pi}} + k_{\text{ri}} \frac{s}{s^2 + \omega_r^2} + \sum_{h=3,5,7} k_{\text{hi}} \frac{s}{s^2 + (h\omega_r)^2} \quad (26)$$

with $k_{\text{pi}} = 7$, $k_{\text{ri}} = 4450$, and $k_{\text{hi}} = k_{\text{ri}}/h$ for $h = 3, 5, 7$; the latter coefficients k_{hi} precautionary decreasing to reduce the impact on the phase margin of the current loop close to the crossover frequency [32]. The PV voltage PI controller is

$$C_v(s) = \frac{k_{\text{pv}}}{s} \left(s + \frac{k_{\text{iv}}}{k_{\text{pv}}} \right) \quad (27)$$

with k_{pv} and k_{iv} chosen around the transfer function (7) at the MPP, setting a target bandwidth of 20 Hz, resulting in $k_{\text{pv}} = 0.05$ and $k_{\text{iv}} = 0.22$. These controllers and the PLL are common to both control schemes. In the proposed scheme of Fig. 5, a unitary gain notch filter removes the double line frequency from the average power calculation; this is

$$h_{\text{notch}}(s) = \frac{s^2 + \omega_o^2}{s^2 + \omega_c s + \omega_o^2} \quad (28)$$

with $\omega_o = 2\pi f_o$ the center angular frequency, and $f_o = 100$ Hz. The bandwidth of $h_{\text{notch}}(s)$ was chosen $\frac{\omega_c}{2\pi} = 85$ Hz to prevent numerical implementation issues [33] and to avoid impacting the average power reference, P_g^* .

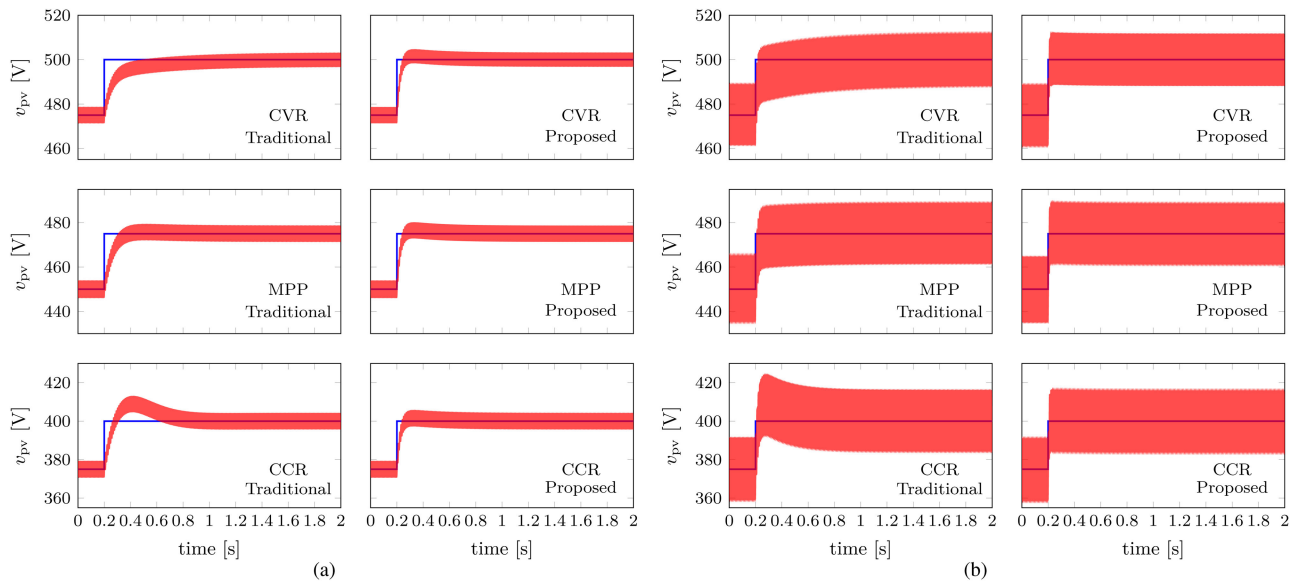


Fig. 7. Simulated PV voltage step response at different operating points of the PV source (CVR, MPP, CCR), for traditional and proposed controller. (a) $C = 1.18 \text{ mF}$. (b) $C = 300 \mu\text{F}$.

A. Transient Performance at Different PV Operating Points

In these simulations, the PV voltage reference is given a 25 V step, and the measured PV voltage is recorded, with the PV source starting from different operating points, that is, on the right of the MPP (CVR, in Fig. 4), at the MPP, and on the left of the MPP (CCR, in Fig. 4). Each test is repeated with two different values of input capacitance, $C = 1.18 \text{ mF}$ and $C = 300 \mu\text{F}$, to additionally investigate the effect of this parameter on the voltage regulation.

The results are presented in Fig. 7, where it is apparent that the transient response with the traditional controller is highly dependent on the PV source operating point. The response is overdamped in the CVR, and becomes under-damped in the CCR, signaling a decreased stability margin, uniquely due to the operating point of the PV source (Fig. 7, left columns).

On the other hand, the proposed PV voltage controller transient performance is independent on the PV source operating point, as the consistency of the plots in Fig. 7 (right columns) indicates. Furthermore, it is noted that a smaller PV side capacitance results in shorter peak and settling times, and a larger PV voltage ripple.

B. PV Voltage Stability Test

In these simulations, the PV voltage reference is decreased in 25 V steps every 3 s, bringing the quiescent point of the PV source from 475 V, located on the right of the MPP (in the CVR), down to 375 V, located on the left of the MPP (in the CCR). This test is carried out twice for each control technique. In the first instance, the voltage controller parameters assume the rated values. In the second instance, the proportional gain of the voltage controller is decreased by 75%, and the effect on the voltage regulation is recorded. As studied in Section III-A, such a dramatic reduction of proportional gain, below the limit given in (15), is expected to expose the closed-loop instability

arising with the conventional controller, when the PV source is operating in the CCR. The results are presented in Fig. 8.

When the PV voltage controller proportional gain assumes its rated value, even though the traditional controller produces a response becoming progressively more underdamped as the PV voltage decreases, the system remains stable [top plots in Fig. 8(a) and (b)]. Conversely, when the voltage controller proportional gain is reduced, the traditional controller fails, as the stability is undesirably dependent on this parameter [bottom plots in Fig. 8(a) and (b)]. With the proposed controller the system remains stable, despite the decreased proportional gain, as the stability is independent of the controller design. These behaviors occur consistently, regardless of input capacitor size.

As observed in Fig. 8(b), the size of the input capacitor is not influencing the stability outcomes, but only the PV voltage ripple and oscillation frequency, therefore this parameter is not changed in the experiments presented next.

V. EXPERIMENTAL RESULTS AND DISCUSSION

A hardware test setup as per Figs. 9 and 10 was implemented to validate the results presented so far. The setup is composed of a 16 kW Regatron PV emulator model TC16.1000.20-Q1-LIN-14050-2 equipped with linear amplifier post-processing unit, emulating the PV source characteristic of Fig. 4; a 50 kVA bidirectional Regatron grid emulator model TC50.480.72-ACS-13039; a 5.5 kW Danfoss converter model FC302-P5K5 with customized protection and interface card; a Texas Instruments TMS320F23879D floating point microcontroller with custom-built input/output interface; ac and dc current and voltage sensors. An isolation transformer was used between the *LCL* filter and the grid emulator for safety reasons, and to isolate the inverter negative bus from the grid emulator ground. The measured signals were displayed on a Yokogawa DLM4000 oscilloscope. The experiments were performed with the same logic and parameters of the simulations (with $C = 1.18 \text{ mF}$).

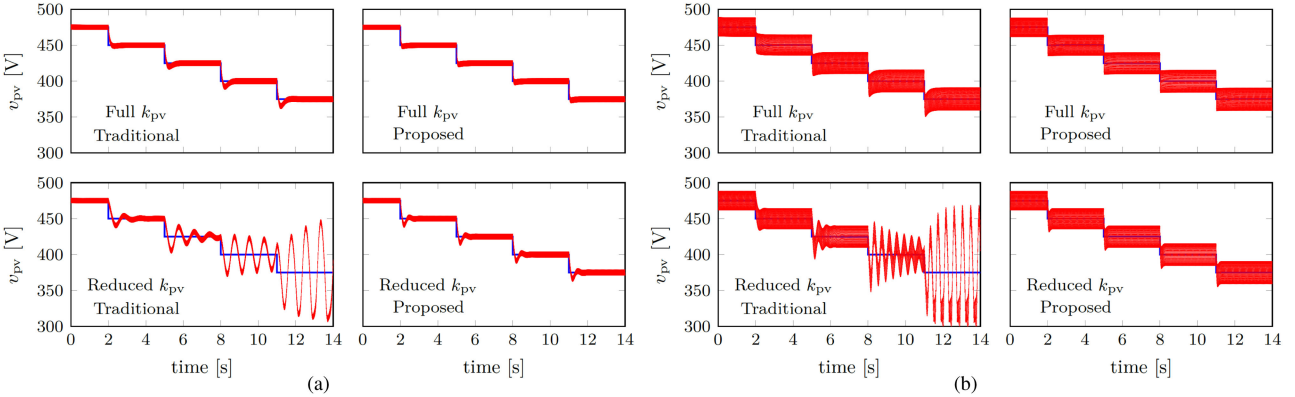


Fig. 8. Simulated PV voltage regulation when the reference is moved from right to left of the MPP in 25 V steps every 3 s. Traditional versus proposed controller with full and reduced k_{pv} . (a) $C = 1.18 \text{ mF}$. (b) $C = 300 \mu\text{F}$.

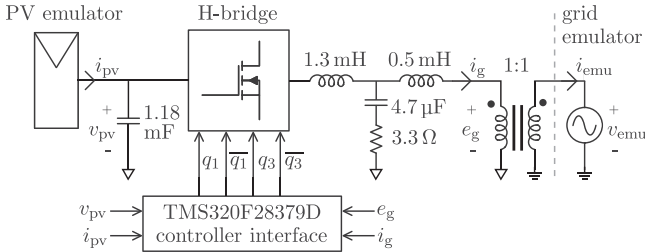


Fig. 9. Experimental setup diagram.



Fig. 10. Actual experimental setup. (1) PV emulator. (2) Cabinet including inverter, LCL filter, μ -controller, and measurements. (3) 1:1 isolation transformer. (4) Grid emulator. (5) PV, grid emulator, and microcontroller software interfaces.

Firstly, the transient performance at different PV operating points is compared. The resulting waveforms from the traditional and the proposed control scheme are reported on the left and right-hand side of Fig. 11, respectively. Although the focus is on the PV voltage regulation, each subfigure also reports the grid current and its reference, for the sake of monitoring the correct operation of the inner current loop.

Fig. 11(a) and (b) refers to a step response when the PV source is operating on the right of the MPP (CVR); Fig. 11(c) and (d) refers to a PV voltage step given about the MPP (450V, in Fig. 4). Finally, Fig. 11(e) and (f) shows the step response when the PV source is working on the left of the MPP (CCR).

Observing Fig. 11(a), (c), and (e), it is apparent that the transient performance with the traditional control technique is inconsistent and heavily dependent on the quiescent point of the PV source, as predicted by the theory and seen in simulation. The step response damping decreases, as the PV source operating point is moved from the CVR [Fig. 11(a)] and MPP [Fig. 11(c)], showing no overshoot, to the CCR [Fig. 11(e)], where the PV voltage step response overshoots, flagging a decreased stability margin. This undesired behavior is due to the pole in (7), which moves depending on the operating point of the PV source, manifested through variations of static and dynamic resistance as in Fig. 4. Recalling Fig. 3, as the plant seen by the voltage controller changes in each operating point of the PV source, so does the transient response. On the other hand, the PV voltage step response from the system controlled with the proposed technique is independent of the PV source operating point, as apparent in Fig. 11(b) (CVR), Fig. 11(d) (MPP), and Fig. 11(f) (CCR), displaying equal transient behavior. This is in accordance with Fig. 6, where the equivalent plant seen by the PI voltage controller does not relate to the operating point of the PV source.

Secondly, the PV voltage regulation stability is assessed for the traditional and proposed control schemes. These tests follow the logic of the simulations in Section IV-B, where the PV voltage characteristic is swept from the right to left of the MPP. Fig. 12(a) and (b) compares the voltage regulation performance between traditional and proposed control schemes, respectively, when the controller parameters assume their rated design value. In the former case [Fig. 12(a)], the lower the PV voltage reference, the more underdamped is the step response, with deteriorating transient performance as the PV voltage moves further to the left of the MPP. On the contrary, this behavior does not occur with the proposed control technique [Fig. 12(b)], where the PV voltage transient response is unaffected by the operating point of the PV source. Fig. 12(c) and (d) refers to results obtained with a voltage controller proportional gain reduced by 75%. This large reduction brings k_{pv} below the critical value given in (15) and, as per the analysis in Section III-A, the PV voltage regulation is expected to become unstable. Accordingly, in Fig. 12(c) the reduced value of k_{pv} causes the traditional controller to fail, when the PV voltage reference moves to the left of the MPP,

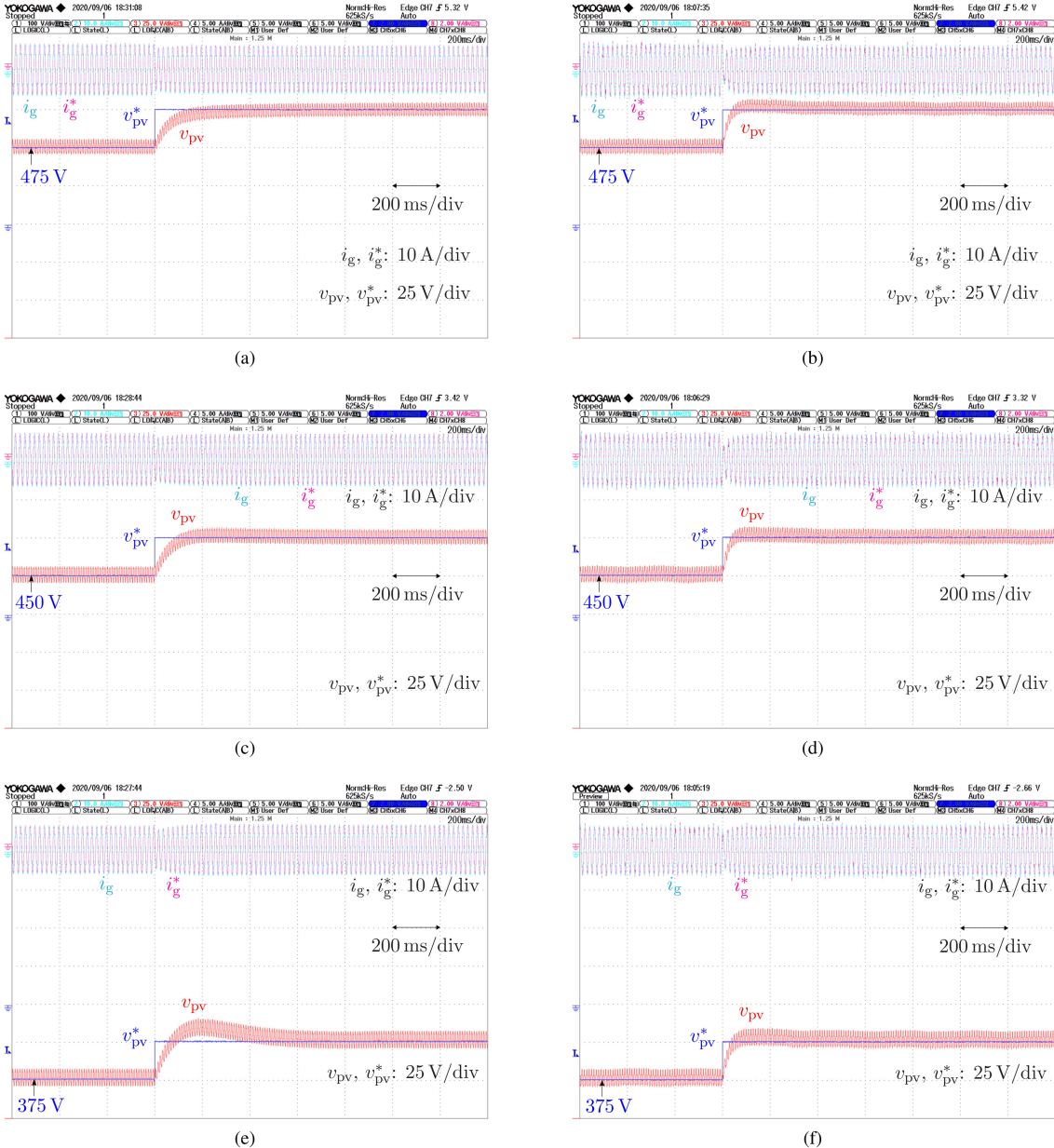


Fig. 11. PV voltage transient behavior when the reference is given a step $\Delta v_{pv}^* = 25$ V at $t = 600$ ms. The PV source quiescent point is moved from the right of the MPP (CVR) to the left of the MPP (CCR), as described. (a) CVR, traditional controller. (b) CVR, proposed controller. (c) MPP, traditional controller. (d) MPP, proposed controller. (e) CCR, traditional controller. (f) CCR, proposed controller.

on the CCR of the I - V curve. Finally, Fig. 12(d) shows the PV voltage transient behavior for the proposed control scheme of Fig. 5, with a reduced value of the outer loop proportional gain, k_{pv} . Despite the challenge of a reduced k_{pv} , the PV voltage regulation remains stable, and independent of the PV operating point, in agreement with the analysis of Section III-B and the simulations of Fig. 8. Although displaying minimal overshoot compared to the case with rated proportional gain in Fig. 12(b), the PV voltage in Fig. 12(d) keeps tracking the reference accurately, and does not become unstable as the PV operating point is moved from the right (CVR) to the left (CCR) of the MPP. In other words, the proposed voltage controller results in a more

robust dynamic performance and superior stability compared to the traditional control scheme.

Finally, it is noted that the experimental waveforms with the proposed controller display a small voltage ripple in Fig. 11(b) and (d), not appearing when the traditional controller is used. This ripple is likely due to noise from measurements introduced in the control loop of Fig. 5, where the PV current is added to the output of the PI voltage controller, C_v , and the result is then multiplied by the PV voltage (performing a nonlinear operation), before entering the notch filter. This set of operations, which on the other hand is not carried out with the traditional controller of Fig. 2, forms the only difference

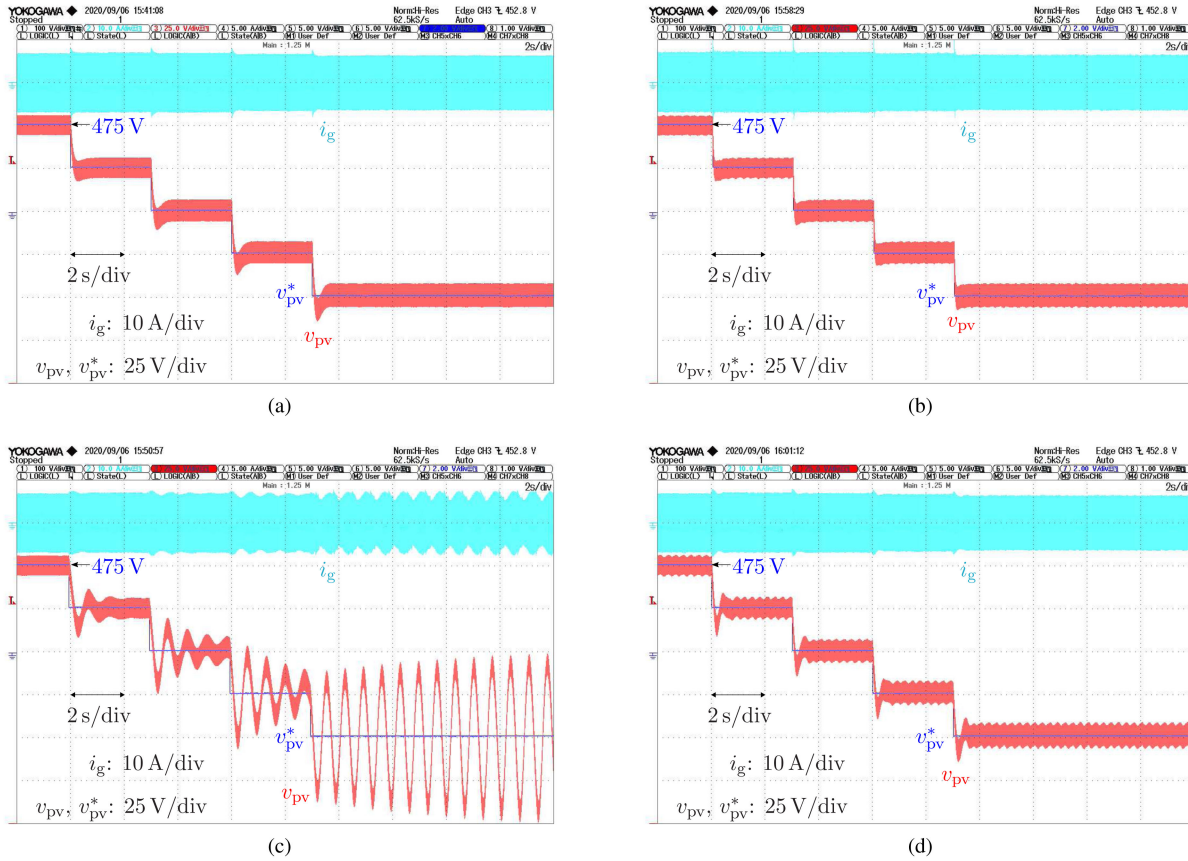


Fig. 12. PV voltage regulation when the PV source I - V curve is swept in steps of $\Delta v_{pv}^* = 25$ V every 3 s. (a) Traditional controller, with rated gain values. (b) Proposed controller, with rated gain values. (c) Traditional controller, k_{pv} reduced by 75% (progressively becomes unstable when the PV source enters the CCR). (d) Proposed controller, k_{pv} reduced by 75%.

between the two schemes. In any case, this ripple is of negligible magnitude and does not affect the validity of the reported findings.

VI. CONCLUSION

This article analyzed the input voltage regulation in the single-stage single-phase PV inverter, taking into account the dynamic model of the PV source. An unstable pole in the plant transfer function describing the PV voltage behavior was demonstrated to have detrimental effects on PV voltage regulation and closed-loop stability, when adopting a traditional linear PV voltage control scheme. In contrast, the proposed PV voltage controller based on feedback linearization resolved these issues. The combination of feed-forward measurements of PV voltage and current to the output of the PI voltage controller, removed the dependence of the PV voltage regulation from the operating point of the PV source, eliminating the closed-loop instability.

In summary, this research produced two main contributions. First, it significantly advanced existing modeling knowledge of single-stage single-phase PV inverters. Second, it produced a new PV voltage control technique, dramatically improving the PV voltage regulation, especially on the left side of the MPP. While this research has unveiled an issue and proposed a solution for it, future work will aim to benchmark the proposed

controller against more advanced PV voltage controllers found in the literature, whose behavior in the CCR has not yet been studied.

REFERENCES

- [1] W. Xiao, N. Ozog, and W. G. Dunford, "Topology study of photovoltaic interface for maximum power point tracking," *IEEE Trans. Ind. Electron.*, vol. 54, no. 3, pp. 1696–1704, Jun. 2007.
- [2] W. Xiao, W. G. Dunford, P. R. Palmer, and A. Capel, "Regulation of photovoltaic voltage," *IEEE Trans. Ind. Electron.*, vol. 54, no. 3, pp. 1365–1374, Jun. 2007.
- [3] T. Suntio, J. Leppäaho, J. Huusari, and L. Nousiainen, "Issues on solar-generator interfacing with current-fed MPP-tracking converters," *IEEE Trans. Power Electron.*, vol. 25, no. 9, pp. 2409–2419, Sep. 2010.
- [4] J. Leppäaho and T. Suntio, "Characterizing the dynamics of the peak-current-mode-controlled buck-power-stage converter in photovoltaic applications," *IEEE Trans. Power Electron.*, vol. 29, no. 7, pp. 3840–3847, Jul. 2014.
- [5] A. Kuperman, M. Sitbon, S. Gadelovits, M. Averbukh, and T. Suntio, "Single-source multi-battery solar charger: Analysis and stability issues," *Energies*, vol. 8, no. 7, pp. 6427–6450, 2015.
- [6] S. Kolesnik, M. Sitbon, S. Gadelovits, T. Suntio, and A. Kuperman, "Interfacing renewable energy sources for maximum power transfer-Part II: Dynamics," *Renew. Sustain. Energy Rev.*, vol. 51, pp. 1771–1783, Nov. 2015.
- [7] S. Gadelovits, M. Sitbon, T. Suntio, and A. Kuperman, "Single-source multibattery solar charger: Case study and implementation issues," *Prog. Photovolt: Res. Appl.*, vol. 23, no. 12, pp. 1916–1928, Dec. 2015.
- [8] L. Callegaro, M. Ciobotaru, D. J. Pagano, and J. E. Fletcher, "Feedback linearization control in photovoltaic module integrated converters," *IEEE Trans. Power Electron.*, vol. 34, no. 7, pp. 6876–6889, Jul. 2019.

- [9] L. Nousiainen *et al.*, "Photovoltaic generator as an input source for power electronic converters," *IEEE Trans. Power Electron.*, vol. 28, no. 6, pp. 3028–3038, Jun. 2013.
- [10] T. Messo, J. Jokipii, J. Puukko, and T. Suntio, "Determining the value of DC-link capacitance to ensure stable operation of a three-phase photovoltaic inverter," *IEEE Trans. Power Electron.*, vol. 29, no. 2, pp. 665–673, Feb. 2014.
- [11] B. Bahrami, A. Rufer, S. Kenzelmann, and L. Lopes, "Vector control of single-phase voltage-source converters based on fictive-axis emulation," *IEEE Trans. Ind. Appl.*, vol. 47, no. 2, pp. 831–840, Mar.-Apr. 2011.
- [12] M. Ebrahimi, S. A. Khajehoddin, and M. Karimi-Ghartemani, "Fast and robust single-phase dq current controller for smart inverter applications," *IEEE Trans. Power Electron.*, vol. 31, no. 5, pp. 3968–3976, May 2016.
- [13] S. Kouro, B. Wu, H. Abu-Rub, and F. Blaabjerg, *Power Electronics for Renewable Energy Systems, Transportation and Industrial Applications*. Chichester, U.K.: Wiley, 2014.
- [14] T. Suntio, T. Messo, and J. Puukko, *Power Electronic Converters: Dynamics and Control in Conventional and Renewable Energy Applications*. Weinheim, Germany: Wiley-VCH, 2018.
- [15] M. Ciobotaru, R. Teodorescu, and F. Blaabjerg, "Control of single-stage single-phase PV inverter," in *Proc. Eur. Conf. Power Electron. Appl.*, 2005.
- [16] L. Nousiainen and T. Suntio, "DC-link voltage control of a single-phase photovoltaic inverter," in *Proc. 6th IET Int. Conf. Power Electron., Mach. Drives*, 2012.
- [17] M. Karimi-Ghartemani, S. A. Khajehoddin, P. Jain, and A. Bakhshai, "A systematic approach to dc-bus control design in single-phase grid-connected renewable converters," *IEEE Trans. Power Electron.*, vol. 28, no. 7, pp. 3158–3166, Jul. 2013.
- [18] R. A. Mastromauro, M. Liserre, and A. Dell'Aquila, "Control issues in single-stage photovoltaic systems: MPPT, current and voltage control," *IEEE Trans. Ind. Informat.*, vol. 8, no. 2, pp. 241–254, May 2012.
- [19] W. Xiao, *Photovoltaic Power System: Modelling, Design and Control*. Hoboken, NJ, USA: Wiley, 2017.
- [20] E. Romero-Cadaval, G. Spagnuolo, L. G. Franquelo, C. A. Ramos-Paja, T. Suntio, and W. M. Xiao, "Grid-connected photovoltaic generation plants: Components and operation," *IEEE Ind. Electron. Mag.*, vol. 7, no. 3, pp. 6–20, Sep. 2013.
- [21] H. D. Tafti, C. D. Townsend, G. Konstantinou, and J. Pou, "A multi-mode flexible power point tracking algorithm for photovoltaic power plants," *IEEE Trans. Power Electron.*, vol. 34, no. 6, pp. 5038–5042, Jun. 2019.
- [22] C. Zhong, Y. Zhou, X.-P. Zhang, and G. Yan, "Flexible power-point-tracking-based frequency regulation strategy for PV system," *IET Renew. Power Gener.*, vol. 14, no. 10, pp. 1797–1807, Jul. 2020.
- [23] M. Liserre, F. Blaabjerg, and S. Hansen, "Design and control of an LCL-filter-based three-phase active rectifier," *IEEE Trans. Ind. Appl.*, vol. 41, no. 5, pp. 1281–1291, Sep./Oct. 2005.
- [24] N. E. Zakzouk, A. K. Abdelsalam, A. A. Helal, and B. W. Williams, "PV single-phase grid-connected converter: DC-link voltage sensorless prospective," *IEEE Trans. Emerg. Sel. Topics Power Electron.*, vol. 5, no. 1, pp. 526–546, Mar. 2017.
- [25] L. Callegaro, M. Ciobotaru, D. J. Pagano, and J. E. Fletcher, "Control design for photovoltaic power optimizers using bootstrap circuit," *IEEE Trans. Energy Convers.*, vol. 34, no. 1, pp. 232–242, Mar. 2019.
- [26] R. Dorf and R. Bishop, *Modern Control Systems*, 12th ed. Upper Saddle River, NJ, USA: Pearson Prentice Hall, 2011.
- [27] J. W. Kolar *et al.*, "Conceptualization and multi-objective optimization of the electric system of an airborne wind turbine," in *Proc. IEEE Int. Symp. Ind. Electron.*, 2011, pp. 32–55.
- [28] A. Urtasun, P. Sanchis, and L. Marroyo, "DC capacitance reduction in three-phase photovoltaic inverters by using virtual impedance emulation," in *Proc. 21st Eur. Conf. Power Electron. Appl.*, 2019.
- [29] N. Nise, *Control Systems Engineering*. Hoboken, NJ, USA: Wiley, 2015.
- [30] M. Ciobotaru, R. Teodorescu, and F. Blaabjerg, "A new single-phase PLL structure based on second order generalized integrator," in *Proc. 37th IEEE Power Electron. Specialists Conf.*, 2006.
- [31] "Software phase locked loop design using C2000 microcontrollers for single phase grid connected inverter," Texas Instruments Inc., Dallas, TX, USA, Appl. Rep. SPRABT3A, Jul. 2017. [Online]. Available: <https://www.ti.com/lit/an/sprabt3a/sprabt3a.pdf>
- [32] M. Schiesser, S. Wasterlain, M. Marchesoni, and M. Carpita, "A simplified design strategy for multi-resonant current control of a grid-connected voltage source inverter with an LCL filter," *Energies*, vol. 11, no. 3, 2018, Art. no. 609.
- [33] M. Maggio, A. Leva, and L. Piroddi, "Finite-precision implementation issues in narrowband active control," in *Proc. 46th IEEE Conf. Decis. Control*, 2007, pp. 1076–1081.



Leonardo Callegaro (Member, IEEE) received the B.Eng. and M.Eng. (hons.) degrees from the University of Padova, Padova, Italy, in 2004 and 2006, respectively, and the Ph.D. degree from The University of New South Wales, Sydney, Australia, in 2018, all in electrical engineering.

He is currently a Lecturer in Electrical Engineering with Macquarie University, Sydney, Australia. His research interests include control for power electronics in photovoltaic energy systems, electric transportation and grid integration of renewables.



Christian A. Rojas (Senior Member, IEEE) was born in Vallenar, Chile, in 1984. He received the Engineering degree in electronic engineering from the Universidad de Concepción, Concepción, Chile, in 2009, and the Ph.D. degree in electronic engineering from the Universidad Técnica Federico Santa María (UTFSM), Valparaíso, Chile, in 2013.

He is currently an Assistant Professor with the Electronic Engineering Department, UTFSM. His research interests include electric transportation, photovoltaic conversion systems, and model predictive control of power converters and drives.

Dr. Rojas is an Associate Editor for the IEEE JOURNAL OF EMERGING AND SELECTED TOPICS IN INDUSTRIAL ELECTRONICS and *IET Power Electronics*.



Mihai Ciobotaru (Senior Member, IEEE) received the Diploma and M.Eng. degrees in electrical engineering from University of Galati, Galati, Romania, in 2002 and 2003, respectively, and the Ph.D. degree in electrical engineering from Aalborg University, Aalborg, Denmark, in 2009.

He currently works as Principal Control Engineer with EcoJoule Energy, Brisbane, Australia, and he also holds an honorary academic position with Macquarie University, Sydney, Australia. His research interests include grid-connected power converters, grid

voltage support, battery energy management systems, microgrids, and renewable energy systems.



John E. Fletcher (Senior Member, IEEE) received the B.Eng. (first-class hons.) and Ph.D. degrees from Heriot-Watt University, Edinburgh, U.K., in 1991 and 1999, respectively, both in electrical and electronic engineering.

From 1998 to 2007, he was a Lecturer with Heriot-Watt University, and from 2007 to 2010, he was a Senior Lecturer with the University of Strathclyde, Glasgow, U.K. He is currently a Professor with the University of New South Wales, Sydney, NSW, Australia. His research interests include power electronics, drives, and energy conversion.

Dr. Fletcher is a Chartered Engineer in the U.K. He is a fellow of the Institution of Engineering and Technology.